Cell

Structure and Subunit Topology of the INO80 Chromatin Remodeler and Its Nucleosome Complex

Alessandro Tosi,[1,2,6] Caroline Haas,[1,2,6] Franz Herzog,[1,2,3,6] Andrea Gilmozzi,[1,2] Otto Berninghausen,[1,2] Charlotte Ungewickell,[1,2] Christian B. Gerhold,[1,2,7] Kristina Lakomek,[1,2] Ruedi Aebersold,[3,5] Roland Beckmann,[1,2,4,*] and Karl-Peter Hopfner[1,2,4,*]

[1]Department of Biochemistry
[2]Gene Center
Ludwig-Maximilian University, 81377 Munich, Germany
[3]Institute of Molecular Systems Biology, Department of Biology, ETH Zürich, 8092 Zürich, Switzerland
[4]Center for Integrated Protein Sciences, 81377 Munich, Germany
[5]Faculty of Science, University of Zürich, 8057 Zürich, Switzerland
[6]These authors contributed equally to this work
[7]Present address: Friedrich Miescher Institute for Biomedical Research, 4058 Basel, Switzerland
*Correspondence: beckmann@genzentrum.lmu.de (R.B.), hopfner@genzentrum.lmu.de (K.-P.H.)
http://dx.doi.org/10.1016/j.cell.2013.08.016

SUMMARY

INO80/SWR1 family chromatin remodelers are complexes composed of >15 subunits and molecular masses exceeding 1 MDa. Their important role in transcription and genome maintenance is exchanging the histone variants H2A and H2A.Z. We report the architecture of *S. cerevisiae* INO80 using an integrative approach of electron microscopy, crosslinking and mass spectrometry. INO80 has an embryo-shaped head-neck-body-foot architecture and shows dynamic open and closed conformations. We can assign an Rvb1/Rvb2 heterododecamer to the head in close contact with the Ino80 Snf2 domain, Ies2, and the Arp5 module at the neck. The high-affinity nucleosome-binding Nhp10 module localizes to the body, whereas the module that contains actin, Arp4, and Arp8 maps to the foot. Structural and biochemical analyses indicate that the nucleosome is bound at the concave surface near the neck, flanked by the Rvb1/2 and Arp8 modules. Our analysis establishes a structural and functional framework for this family of large remodelers.

INTRODUCTION

ATP-dependent chromatin remodelers use the energy of ATP hydrolysis to regulate or facilitate DNA-associated processes by sliding nucleosomes, evicting histones, or exchanging histone variants (Papamichos-Chronakis and Peterson, 2013; Seeber et al., 2013). Remodelers are grouped into four major families: SWI/SNF, INO80/SWR1, ISWI, and CHD/Mi-2 (Clapier and Cairns, 2009). They all possess a Snf2-type ATPase but are otherwise diverse in their structural composition and biochemical activity (Hopfner et al., 2012).

The INO80 complex is implicated in transcription (Shen et al., 2000), replication (Papamichos-Chronakis and Peterson, 2008), cell division, and DNA repair (Downs et al., 2004; Morrison et al., 2004; van Attikum et al., 2004) and catalyzes the exchange of H2A.Z/H2B dimers with free H2A/H2B (Papamichos-Chronakis et al., 2011). The reverse reaction, the incorporation of H2A.Z is catalyzed by the related SWR1 complex (Mizuguchi et al., 2004), and both complexes regulate the global distribution of H2A.Z with emerging implications in genomic stability, cancer development, and embryonic stem cell differentiation (Billon and Côté, 2012; Li et al., 2012).

The INO80 complex has a molecular mass of 1.3 MDa and is composed of 15 different subunits in *Saccharomyces cerevisiae*: Snf2 ATPase Ino80, AAA^+ ATPases Rvb1 and Rvb2, *a*ctin-*r*elated-*p*rotein (Arp4), Arp5 and Arp8, Act1 (actin), *T*BP-*a*ssociated *f*actor 14 (Taf14), *non*histone *p*rotein 10 (Nhp10), and *I*no *e*ighty *s*ubunits 1–6 (Ies1–Ies6) (Shen et al., 2000, 2003). Ino80 could act as DNA translocase in remodeling but has also scaffold functions. Metazoan-specific subunits bind the N terminus of human Ino80, whereas Arp5, Ies6, Ies2, and Rvb1/2 interact with its C-terminal Snf2 domain of Ino80 (Chen et al., 2011; Jónsson et al., 2004). Recruitment of Rvb1/2 requires a characteristic insertion in the Snf2 domain of INO80/SWR1 remodelers (Wu et al., 2005).

Rvb1/2 are essential for the remodeling activity of INO80 (Jónsson et al., 2004), but their function remains unclear (Jha and Dutta, 2009). Actin, Arp8, and Arp4 form a structural module with the central *h*elicase *S*ANT-*a*ssociated (HSA) domain of Ino80 and function in histone or nucleosome interactions (Gerhold et al., 2012; Harata et al., 1999; Saravanan et al., 2012; Schubert et al., 2013; Shen et al., 2003; Szerlong et al., 2008). Arp5, Arp8, Ies4, and Nhp10 are implicated in DNA repair (Morrison et al., 2004, 2007; van Attikum et al., 2004). The *h*igh

*m*obility *g*roup (HMG) protein Nhp10 binds preferentially distorted or supercoiled DNA (Ray and Grove, 2009) and is physically associated with Ies3 (Morrison et al., 2004; Shen et al., 2003). Taf14, a subunit that is shared by several DNA-interacting complexes, contains a YEATS domain that shows similarities to the histone chaperone Asf1 (Schulze et al., 2010; Wang et al., 2009).

A major obstacle in understanding the mechanism of INO80 is the lack of structural frameworks. SWI/SNF family remodelers and a RSC nucleosome complex were visualized by electron microscopy (EM) (Asturias et al., 2002; Chaban et al., 2008; Dechassa et al., 2008; Leschziner et al., 2005, 2007; Skiniotis et al., 2007; Smith et al., 2003), but the current information does not go beyond overall shapes. No structural information is available for an INO80-type complex, and only some subunits have been characterized structurally: isolated Rvb1/2 (Gorynia et al., 2011; López-Perrote et al., 2012; Matias et al., 2006; Puri et al., 2007; Torreira et al., 2008), the YEATS domain of Taf14 (Zhang et al., 2011), actin (Vorobiev et al., 2003), Arp4, and Arp8 (Fenn et al., 2011; Gerhold et al., 2012; Saravanan et al., 2012).

To establish a structural framework for INO80, we used a hybrid structural biology approach that combines cryo-EM and single particle three-dimensional (3D) reconstruction with chemical crosslinking and mass spectrometry (XL-MS) (Herzog et al., 2012). Our analysis revealed that INO80 consists of 25 subunits, including a Rvb1/2 dodecamer, organized in four modules (head-neck-body-foot) in an elongated structure. We place the Rvb1/2 dodecamer and the Snf2 domain in the electron density and map subcomplexes to structural modules using *d*ynein light chain-*i*nteracting *d*omain (DID) labeling (Flemming et al., 2010). Furthermore, we mapped interactions of INO80 to the nucleosome and visualized INO80 nucleosome complexes by EM and two-dimensional (2D) class averaging. Our results indicate that INO80 is structurally and mechanistically distinct from SWI/SNF-type remodelers, and instead of providing a nucleosome-binding pocket, INO80 forms a flexible clamp in histone variant exchange and nucleosome remodeling.

RESULTS

3D Structure of the INO80 Complex

We purified the 1.3 MDa INO80 complex from *S. cerevisiae* to near homogeneity (Figures S1A and S1B available online) and validated activity by an ATP-dependent remodeling assay (Figure S1C). In order to determine a structure of INO80, we recorded electron micrographs of negatively stained specimen (Figure S1D). Particles were selected manually and classified reference free using EMAN2 (Tang et al., 2007) and iterative and stable alignment and clustering (ISAC) (Yang et al., 2012). Stabilization of INO80 by mild crosslinking preserved overall features and improved particle quality (Figure S1E). Common line reconstruction from classes of both 2D classification methods resulted in very similar initial 3D models (Figure S1F) and were used for further refinement of the 3D structure to a resolution of 22 Å (Figures 1A, 1B, and S1G). The negative-stain 3D structure was filtered to 35 Å and used as an initial reference for determination of a cryo-EM structure to a resolution of 17 Å (Figure 1C and S1G).

In general, class averages were in good agreement with projections of the refined 3D EM structure (Figures 1B and S1E). However, a small subset of stable classes derived from reference-free classification by ISAC could not be assigned to a projection of the refined, elongated EM structure of INO80 and showed rather bent conformations (Figure 1B), indicating conformational flexibility in INO80.

Negative-stain and cryo-EM structures of INO80 reveal an asymmetric, embryo-shaped particle that consists of a globular head that is connected to a body and foot via a neck (Figures 1A and 1C). The overall dimensions are 310 × 210 × 160 Å. The globular head has a diameter of ~120 Å and represents approximately half of the volume of INO80. It is positioned laterally on one end of the cone-shaped neck-body-foot structure, creating a sharp kink in INO80 with a prominent groove. Notably, the flexibility in the foot observed in bent class average of negatively stained particles is reflected in lower resolution of the foot compared to the remainder of INO80 (Figure S1H).

The elongated structure of INO80 is remarkably different from the EM structures of SWI/SNF and RSC remodelers (Leschziner, 2011), which contain a central cavity that has been shown to bind the nucleosome (Chaban et al., 2008). INO80 has no such cavity, suggesting a different mode of interaction with nucleosomes. The observed flexibility of the foot indicates that the INO80 can undergo substantial conformational changes that could be part of nucleosome recognition or remodeling.

In summary, our data establish an overall structure of INO80 that reveals a distinct elongated, modular shape and the potential for large-scale conformational changes.

The Head of the INO80 Complex Contains an Rvb1/2 Heterododecamer

Because of its size and shape, the head is the only candidate for the distinctive Rvb1/2 AAA^+ ATPases. We analyzed the rotational cross-correlation of the head volume around its axis and detected a 6-fold symmetry (Figures 1D and S1I). This symmetry with its axis oriented approximately parallel to the neck-body-foot cone strongly suggests that the head indeed harbors the Rvb1/2 complex. The symmetry axis allows us to orient the AAA+ fold and also validates the quality of the electron density.

The shape and volume of the head (~600 kDa) are consistent with a dodecamer, but not a hexamer, of Rvb1/2. A Rvb1/2 dodecamer in the form of two stacked hexamers derived from crystal structures of the human orthologs (Gorynia et al., 2011; Matias et al., 2006) can be placed into the head of the EM density (Figure 1E). The overall shape of the averaged head (Figure 1F) also matches isolated Rvb1/2 dodecamers, although the Rvb1/2 rings are more compact in the INO80 complex than in any isolated structure (López-Perrote et al., 2012). It is possible that a particular conformation of Rvb1/2 is stabilized in INO80, consistent with the notion that AAA+ ATPases can undergo substantial conformational rearrangements during their ATP-dependent functional cycle. Our analysis suggests that Rvb1/2 forms a distinct peripheral module—rather than an integral structural component—in INO80.

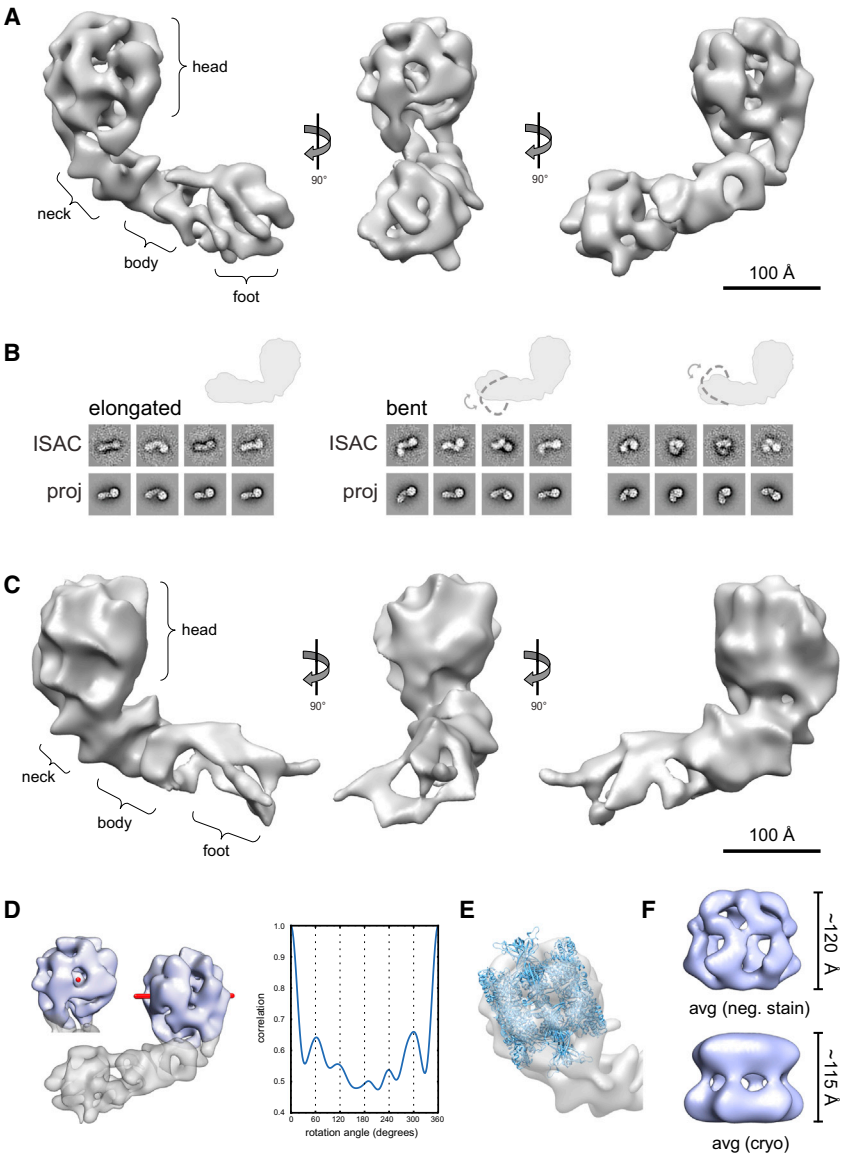

Figure 1. 3D Structure of the INO80 Complex

(A) The 3D electron density map of INO80 from negative staining has an elongated embryo-like shape with four modules: a globular head connected via a neck to the body and foot. The bar represents 100 Å.

(B) Conformational flexibility. Reference-free class averages from ISAC were correlated to projections of the INO80 complex. Elongated classes match the projections, whereas bent classes diverge from the elongated model.

(C) The cryo-EM structure is similar to the negative-stain structure.

(D) The 6-fold symmetry in the head of INO80 proves the location of the Rvb1/2 complex. The symmetry axis (red) is quasiparallel to the residual cone of INO80. Cross-correlation of the Rvb1/2 head rotated along the axis harbors six maxima, spaced by 60°.

(E) The dimensions of the head are suited to dock two hexameric human Rvb1 rings (PDB ID code 2C9O; Matias et al., 2006).

(F) Electron density maps of an averaged Rvb1/2 head with applied 6-fold symmetry reveal two asymmetric hexameric rings.

See also Figure S1.

Subunit Interaction Topology and Structural Modules from Crosslinking and Mass Spectrometry

With the overall 3D structure of INO80 in hand, we determined a subunit interaction map with motif resolution using chemical crosslinking and mass spectrometry (Herzog et al., 2012). In four experiments, we identified 534 intralinks (crosslinks within the same polypeptide) (Table S1) and 217 interlinks (crosslinks between two polypeptides) (Table S2). This resulted in a set of 212 or 116 unique intra- or interlinks, respectively (Figure 2). Intralinks on available crystal structures or homology models fulfilled the distance restraint of ≤30 Å (Herzog et al., 2012), validating our approach (Tables S1 and S2).

We identified four topological modules in addition to an Ino80-Ies2 scaffold: Nhp10-Ies1-Ies3-Ies5 (Nhp10-module), Arp4-Arp8-Act1-Taf14-Ies4 (Arp8-module), Rvb1-Rvb2 (Rvb1/2 module), and Arp5-Ies6 (Arp5-module) (Figure 2). These results are in agreement with prior biochemical studies on the modular architecture of INO80 (Chen et al., 2011; Jónsson et al., 2004; Szerlong et al., 2008).

The Nhp10 module consists of Nhp10, Ies1, Ies3, and Ies5. These yeast-specific subunits crosslinked to the N terminus of Ino80 and formed a stable complex in vitro (Figures S2E and S2F). Metazoan-specific subunits require the N terminus of human Ino80 to be recruited to INO80, implying a conserved functional architecture of INO80 (Chen et al., 2011).

The Arp8 module comprises the evolutionary conserved subunits Act1, Arp4, and Arp8 at the HSA domain, as observed (Szerlong et al., 2008), but also includes Ies4 and Taf14. Indeed, we could purify a stable complex of HSA^{Ino80}, Act1, Arp4, Arp8, and Ies4 (Figure S2G). The majority of the observed crosslinks were between the N-terminal domain of Arp8 (outside the actin fold) and the region just N-terminal to the HSA domain (Figure 2). This region of Ino80 also crosslinked to Ies4, Arp4, and Taf14.

The Rvb1/2 module contained Rvb1 and Rvb2, and the Arp5 module contained Arp5 and Ies6. Both Rvb1 and Rvb2 crosslinked to the Ino80 insertion, compatible with Rvb1/2's recruitment to SWR1 via the insertion of Swr1 (Wu et al., 2005). We found nine unique crosslinks between Rvb1 and Rvb2 and validated the Arp5-Ies6 interlinks by purifying a stable Arp5-Ies6 complex (Figure S2H). Ies6 exclusively crosslinked to domain 2 of Rvb2, whereas Arp5 crosslinked exclusively to Ies6. This is consistent with an ATP-modulated interaction of Arp5-Ies6 with Rvb1/2 (Jónsson et al., 2004).

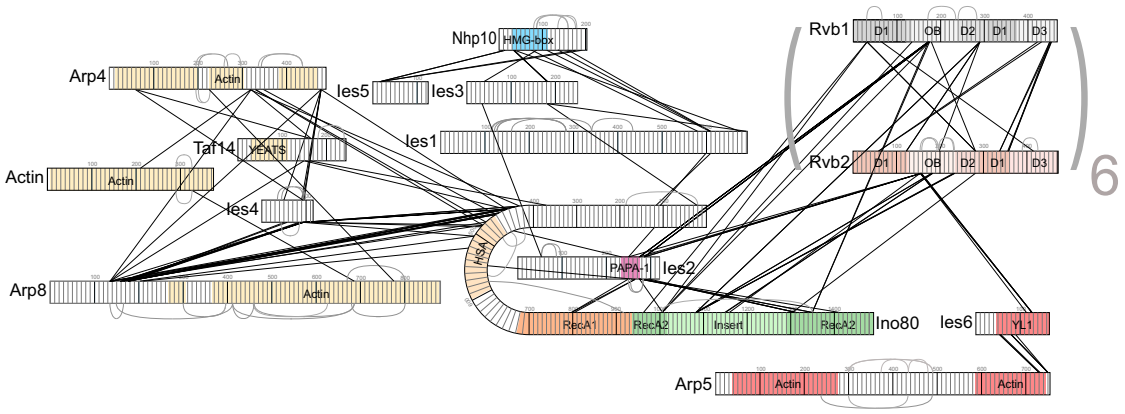

Figure 2. Topology of the INO80 Complex

XL-MS analysis revealed the interaction map of INO80 subunits. Interlinks are depicted in black. Intralinks with a minimum of 30 amino acids between linkage sites are shown in gray. Ino80 (HSA, dark yellow; RecA1, orange; RecA2, green; insertion, light green) and Ies2 (pink) serve as scaffolds for the subcomplexes Arp4, Arp8, Act, Ies4, and Taf14 (yellow); Nhp10 (blue), Ies1, Ies3, and Ies5; Rvb1 (gray), Rvb2 (coppery), Arp5, and Ise6 (red).

See also Figure S2 and Tables S1 and S2.

Ies2 has a special structural role. It is conserved between species, and we found interlinks between its uncharacterized PAPA-1 domain not only to domains 2 of both Rvb1 and Rvb2 but also to Ies3 of the Nhp10-module and to regions along Ino80's entire polypeptide chain. All of these crosslinks mapped to a short region on Ies2, suggesting that Ino80 is not highly extended in the INO80 complex but rather folds back.

In summary, we provide a comprehensive subunit interaction topology that is consistent with, and substantially extends, prior studies on the modular architecture of INO80, especially bringing in a new quality with domain and motif resolution of the interactions.

Biochemical Validation of Structural Modules

Whereas the copurification analysis validated the modules identified by the crosslinks in vitro, we validated the modular organization also in vivo by purification of INO80 complexes from *Δarp5*, *Δarp8*, or *Δnhp10* strains and analysis of subunit composition by SDS-PAGE and MS analysis (Figures 3A and 3B; Tables S3 and S4). Our data agree with previous observations (Chen et al., 2011; Shen et al., 2003), but with an expanded loss of further subunits. INO80(Δnhp10) lacked Ies1, Ies3, and Ies5, whereas INO80(Δarp8) lacked Arp4 and Ies4 and showed reduced levels of Taf14 and Act1. In contrast, deletion of Arp5 had no effect on other subunits, except Ies6, which was missing.

In conclusion, these data are fully consistent with, and further validate, the XL-MS defined modules.

The Rvb1/2 Dodecamer

Using the subunit topology of INO80 from XL-MS, we are able to extend the interpretation of the 3D EM structure. Rvb1/2's monomers consist of three domains (Matias et al., 2006). Domain 2 with oligonucleotide binding (OB) folds intersperses the AAA+ ATPase that is formed by domains 1 and 3. We built a molecular model of a yeast dodecameric Rvb1/2, using the crystal structures of human hexameric Rvb1 (Matias et al., 2006) and dodecameric Rvb1/2 (with deleted OB folds) (Gorynia et al., 2011) on the basis of their 70% sequence identity (Figure 4A).

Isolated Rvb1/2 dodecamers can theoretically adopt different stacking arrangements via AAA+ domains 1/3 and/or domain 2: (1) 2-2, (2) 1/3-2, or (3) 1/3-1/3 (Figure S3A). We assembled six Rvb1/2 models—homo- versus heterohexamers—in all possible stacking orientations and analyzed the available nine interlinks between Rvb1 and Rvb2. These crosslinks were exclusively consistent with two stacked, alternating heterohexamers, but disfavored two stacked homohexamers (Figures 4A and 4B; Figures S3A and S3B).

To determine how the two heterohexameric rings stacked, we analyzed monolinks that are indicative of solvent accessibility (lysine residues that are modified by disuccimidyl suberate [DSS], but not crosslinked) (Figure 4C; Table S5). We found monolinks on ~80% of lysines on the convex side of the Rvb1/2 heterohexamer but only on ~10% of lysines on the concave side, suggesting that the convex surface is solvent exposed in the dodecamer, whereas the concave surface is more secluded (Figure 4C).

In summary, our data indicate two heterohexameric Rvb1/2 rings stacked with the AAA+ domains 1 and 3 at the poles and the OB fold domains 2 at the equatorial plane. Using the symmetry axis in the head, the equatorial plane with its OB fold belt points toward the neck.

The Snf2 Domain

Multiple crosslinks between Rvb1/2—in particular, domain 2—and the Snf2 domain of Ino80 indicate that the Snf2 domain must be located at the neck (Figure 2). Significantly, the neck harbors a density patch in the EM map that showed the characteristic two-lobed shape of Snf2 domains (Figures 1A and 1C) (Dürr et al., 2005; Thomä et al., 2005). The *Danio rerio* (*Dro*) Rad54 Snf2 domain, a homolog of the Ino80 Snf2 domain for which a crystal structure is available (Thomä et al., 2005), fit well into the density at the neck with a cross-correlation

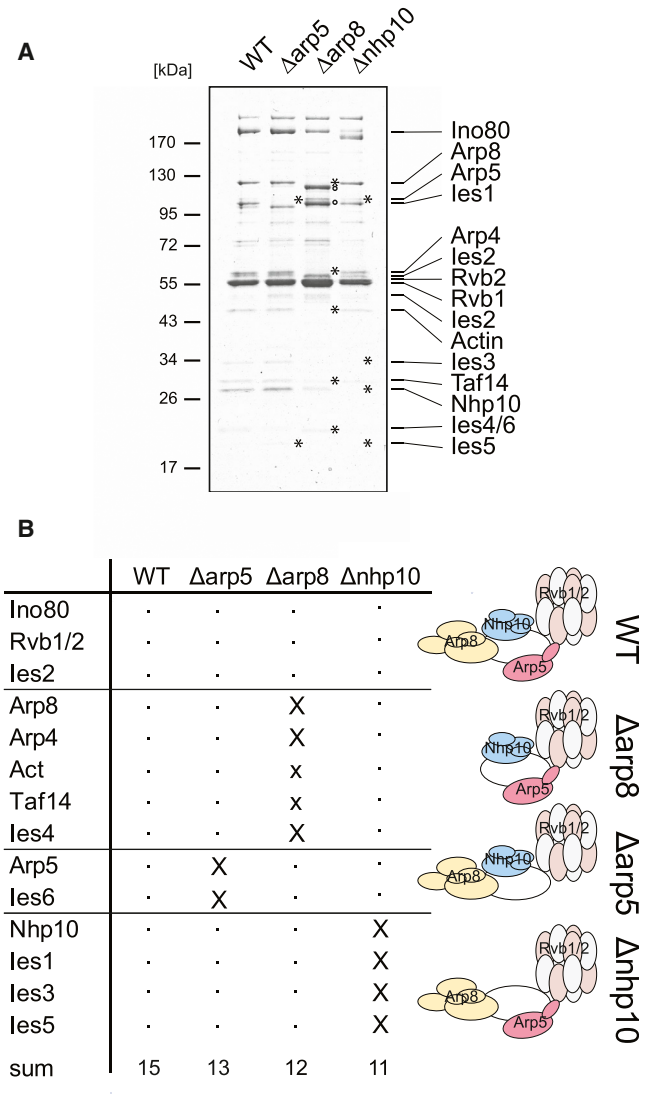

Figure 3. The Modular Architecture of INO80

(A) Coomassie-stained SDS-PAGE of INO80 FLAG-purified complexes from WT and deletion mutants: *Δarp5*, *Δarp8*, and *Δnhp10*. Missing and reduced subunits are indicated with an asterisk. INO80(Δarp8) showed inferior purity and degradation products of Ino80 (circles).

(B) Comparison of the subunit compositions of mutant and WT INO80 complexes. Presence (dot), absence (X), or decreased levels (x) of subunits within INO80 complexes were analyzed by MS and SDS-PAGE.

See also Tables S3 and S4.

coefficient of 0.87 (Figure 4D). The docked orientation was further constrained by and is in agreement with several interlinks of Rvb1/2 to the RecA2 lobe of the Ino80 Snf2 domain. In this orientation, density connecting the head with neck could harbor the 30 kDa Ino80 insertion loop of the RecA2 lobe (Figure 4D). Additional density on top of Ino80's ATPase could harbor the Ies2 PAPA-1 domain that crosslinks to RecA1 and RecA2 domains of Ino80 and the OB fold domains of Rvb1/2. A groove between head and neck could potentially accommodate nucleosomal DNA, bound at the Snf2 domain (see below). The DNA binding domains of Rvb1/2 and the Ino80 ATPase are in close proximity and could consequently act on DNA in a coordinated manner.

Taken together, our hybrid approach allowed us to place the Snf2 domain at a central region of INO80 and suggested a structural and possibly functional interaction of both Rvb1/2 and Ino80 ATPases.

Localization of Arp8, Nhp10, and Arp5 Modules

In order to position the Arp8 module in INO80, we performed DID labeling (Flemming et al., 2010) of Arp4 as a representative of the module. By negative-stain EM, we found the DID-tag protruding from the foot of INO80 (Figure 5A). The lack of crosslinks of the Arp8 module to other modules is also consistent with this peripheral position.

To localize the Nhp10 module, we visualized INO80 DID tagged at Nhp10 and found the tag protruding out of the body (Figure 5A). The volume of the body of INO80 fits well with this finding. The more central location of the Nhp10 module was already indicated by crosslinks of Ies3 to Ies2 (Figure 2).

The Arp5 module was localized using a DID-tag on its interaction partner Ies6, which we found at the neck (Figure 5A). This location is in agreement with crosslinks of Ies6 to Rvb2 (Figure 2). The EM map shows an unaccounted density at this part of the neck region that matches well to an actin fold (Figure S4A).

Finally, we labeled Ies2 and found the DID-tag also protruding near the neck (Figure 5A), in good agreement with its proposed location at the top of the Snf2 fold from the crosslink analysis (Figures 2 and 4D).

In summary, the combination of EM, XL-MS, and DID-tagging suggests the following INO80 subunit topology: head, Rvb1/2 module; neck, Ino80 ATPase, Ies2, and Arp5 module; body, Nhp10 module; and foot, Arp8 module (Figure 5B).

Functional Analysis of Structural Modules

To reveal the role of different modules in nucleosome remodeling, we tested INO80 from wild-type (WT), *Δarp8*, *Δnhp10*, and *Δarp5* strains with respect to DNA and nucleosome binding, nucleosome sliding, and DNA or nucleosome-stimulated ATPase activity. All three INO80 deletion variants still bound nucleosomes and DNA, indicating multiple contacts between the remodeler and the nucleosome (Figures 5C and S4B). INO80(Δarp5) showed marginally reduced binding affinities toward DNA and nucleosomes but was not able to redistribute nucleosomes (Shen et al., 2003) (Figures 5C, 5D, and S4B). Recombinant Arp5-Ies6 bound DNA with moderate affinity, whereas nucleosomes were not bound in our assays (Figures S4C–S4E). DNA stimulated the ATP hydrolysis of INO80(Δarp5) comparable to that of WT INO80. Nucleosomes, however, did not further increase activity, in contrast to WT INO80 (Figure 5E).

The lack of the Arp8 module negatively influenced, but did not completely abolish, binding to nucleosomes and DNA and the remodeling activity of INO80(Δarp8) as observed in Shen et al. (2003) (Figures 5C, 5D, and S4B). Consistently, recombinant HSA-Act-Arp4-Arp8 binds DNA and nucleosomes (Figures 5F, S4C, and S4F). Furthermore, the ATPase activity of INO80(Δarp8) was not stimulated by DNA (Figure 5E); however, nucleosomes increased the ATPase activity equivalent to that

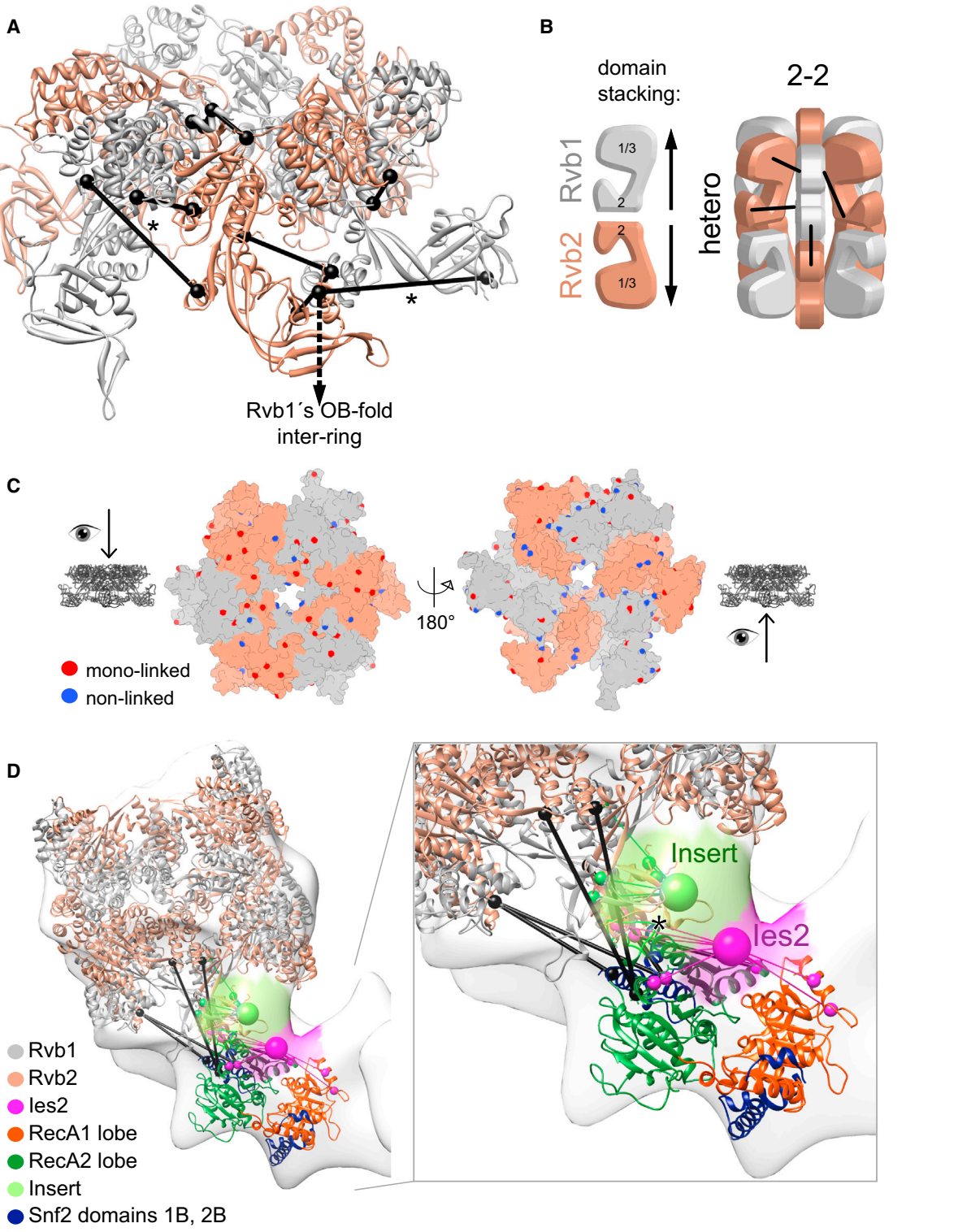

Figure 4. The Rvb1/2 Complex and the Snf2 Domain in INO80

(A) Crosslinks (black) found between the ATPase domains 1/3 and domains 2 of Rvb1 (gray) and Rvb2 (coppery) restrained the topology of the Rvb1/2 complex to a heterohexameric arrangement. Crosslinks in flexible regions are marked by asterisks (see also Figure S3B).

(B) Of all possible stacking arrangements of Rvb1/2's rings (see Figure S3A), a domain 2-2 stacking of heterohexamers exclusively fulfilled the crosslinks (black).

(C) Solvent accessibility of the convex side of the Rvb1/2 rings was indicated by monolinked lysines (red), whereas lysines at the concave side were predominantly nonmodified (blue), suggesting that rings of Rvb1/2 face each other with the domains 2 at the concave side.

(legend continued on next page)

of WT INO80 in the presence of DNA. The Arp8 module has been suggested to be associated with extranucleosomal DNA (Kapoor et al., 2013) and histones (Gerhold et al., 2012; Harata et al., 1999; Saravanan et al., 2012; Shen et al., 2003) and may detect both in the remodeling reaction.

In contrast to the nucleosome and DNA binding proficient and remodeling deficient Arp5 and Arp8 deletions, INO80(Δnhp10) showed substantially reduced DNA and nucleosome binding but proficient remodeling (Shen et al., 2003) (Figures 5C, 5D, and S4B). In agreement, recombinant Nhp10-Ies3-Ies5 tightly bound to DNA and nucleosomes (Figures 5F, S4C, and S4F), suggesting that this module helps high-affinity targeting of INO80. However, the Nhp10 module had no influence on the intrinsic or stimulated ATPase activity and the capability to reposition nucleosomes, suggesting that it is not part of the core remodeling activity (Figure 5E).

In summary, these data suggest that Arp8 and Arp5 modules participate in the remodeling reaction, whereas the Nhp10 module contributes to high-affinity DNA or nucleosome recognition.

Interaction of INO80 with the Nucleosome

To map the histone interaction sites of INO80, we analyzed a complex reconstituted from INO80 and a nucleosome by XL-MS (Figure S5A). We found 52 interlinks (Table S6; Figures 6A and 6B; Figures S5B and S5C) of INO80 subunits to histones of the nucleosome (*Drosophila melanogaster*, Protein Data Bank [PDB] ID code 2PYO; Clapier et al., 2008). Thirty-five crosslinks were formed to the flexible histone tails, representing only loose distance restraints. However, 17 interlinks between structured parts of the histones and INO80 subunits enabled us to approximately position the nucleosome on INO80.

All four modules crosslinked to all four histones: 12 crosslinks of the Rvb1/2 head, 14 of the Ino80 ATPase-Ies2-Arp5-Ies6 neck, 10 of the Ino80 N-term-Nhp10-Ies1-Ies3-Ies5 body, and 16 of the foot containing the Ino80 HSA-Act1-Arp4-Arp8-Ies4-Taf14 (Figures 6A and 6B; Figures S5B and S5C). Because INO80/SWR1-type remodelers are suggested to catalyze exchange of H2A/H2B and H2A.Z/H2B dimers (Morrison and Shen, 2009; Papamichos-Chronakis et al., 2011), how INO80 subunits interact with the exchanged H2A (or H2A.Z) and H2B in comparison with the nonexchanged H3 and H4 is of particular interest. The Rvb1/2 dodecamer crosslinked to residues in N and C termini of H2A, the N terminus, helices α2 and αC of H2B, the N terminus of H3, the N terminus, and the loop (L1) between helices α1 and α2 of H4 spanning one side of the nucleosome (gray). The Ino80 ATPase (RecA2 lobe) crosslinked to the loop insertion between α2 and α3 (L2) of H2A, and the insertion of RecA2 crosslinked to the N terminus of H3. Ies2 crosslinked to helix α1 of H3 and to αC of H2B, as well as to the N termini of H2A, H2B, and H4. Arp5-Ies6 crosslinked to the αC helix of H2B, L1 of H4, and to the N termini of H2B and H3. The Nhp10 module, including the N terminus of Ino80, crosslinked to α1 and α2 helices of H4, αC of H2B, and to all the N termini of histones. The Arp8 module containing the HSA domain crosslinked to αC helix of H2B, L2 of H2A, and the N termini of all histones. The involvement of all modules in core histone fold crosslinks strongly argued for a central position of the nucleosome within INO80.

The crosslinks of the H2A and H2B core secondary structures to RecA2, Arp5/Ies6, Ies2, and Rvb1/2 domains 2 suggested that the H2A/H2B dimer is located near the neck of INO80 and raised the possibility that an ATP-dependent chemomechanical activity of the Snf2 domain could loosen contacts between DNA and exchanged histones. Interestingly, the location of the RecA2 crosslink coincides with the binding site of ISW2 on the nucleosome (Dang and Bartholomew, 2007). We also noticed that some lysines involved in crosslinks among Ies2 and helix α1 of H3, Rvb2 to helix α2 of H2B and Ies6 as well as Rvb2 to L1 of H4 are not surface exposed in an intact nucleosome. Such interactions would require partial unwrapping of the DNA at the entry/exit site, possibly additionally helping to create an accessible H2A/H2A.Z for exchange.

To directly visualize the nucleosome on INO80, we analyzed negatively stained particles of INO80 bound to nucleosomes. Stable class averages from ISAC (Yang et al., 2012) showed additional density at the central groove that is not visible on corresponding projections of INO80 alone (Figure 6C). This position was consistent with the central location predicted from the crosslinking analysis. The highly dynamic nature of INO80, insufficient occupancy, and possibly partial remodeling of the nucleosome prevented robust 3D reconstruction of this complex so far.

A model for the INO80 nucleosome complex on the basis of crosslinks and EM is shown in Figure 7.

DISCUSSION

We provide the architectural framework of the INO80 chromatin remodeler and its interaction with a nucleosome using an integrative structural approach. One unexpected result is that the elongated structure of INO80 is distinct from available structures of the SWI/SNF family of large (>1 MDa) remodelers (Leschziner, 2011). The latter showed a C-shaped/globular structure with a central nucleosome-binding cavity. RSC remodelers are able to completely engulf nucleosomes (Chaban et al., 2008), whereas the binding site of SWI/SNF suggests an only partial envelopment (Dechassa et al., 2008). In contrast, INO80 contains no apparent nucleosome-binding cavity but forms a suitable cradle (Figure 7). Because assignment of density to subunits or modules has not been reported for SWI/SNF-type remodelers yet, a more in-depth structural comparison and correlation of structural features to different biochemical activities must await progress on their architecture. Limited by their size, small ISWI remodelers have only few contacts to the

(D) *Dro* Rad54 (Thomä et al., 2005) related to the Snf2-fold of Ino80 was docked into the neck region of the INO80 EM density and oriented by crosslinks (black) to Rvb1/2. Small spheres represent lysines of RecA1, RecA2 of Ino80, and OB folds of Rvb1/2 that crosslinked to either Ies2 (pink) or the insertion of Ino80 (light green). Ies2 was localized at the top of Snf2 fold (pink ball). The remaining density at the neck (light green ball) may harbor the insertion that protrudes out of RecA2 (asterisk).
See also Figure S3 and Table S5.

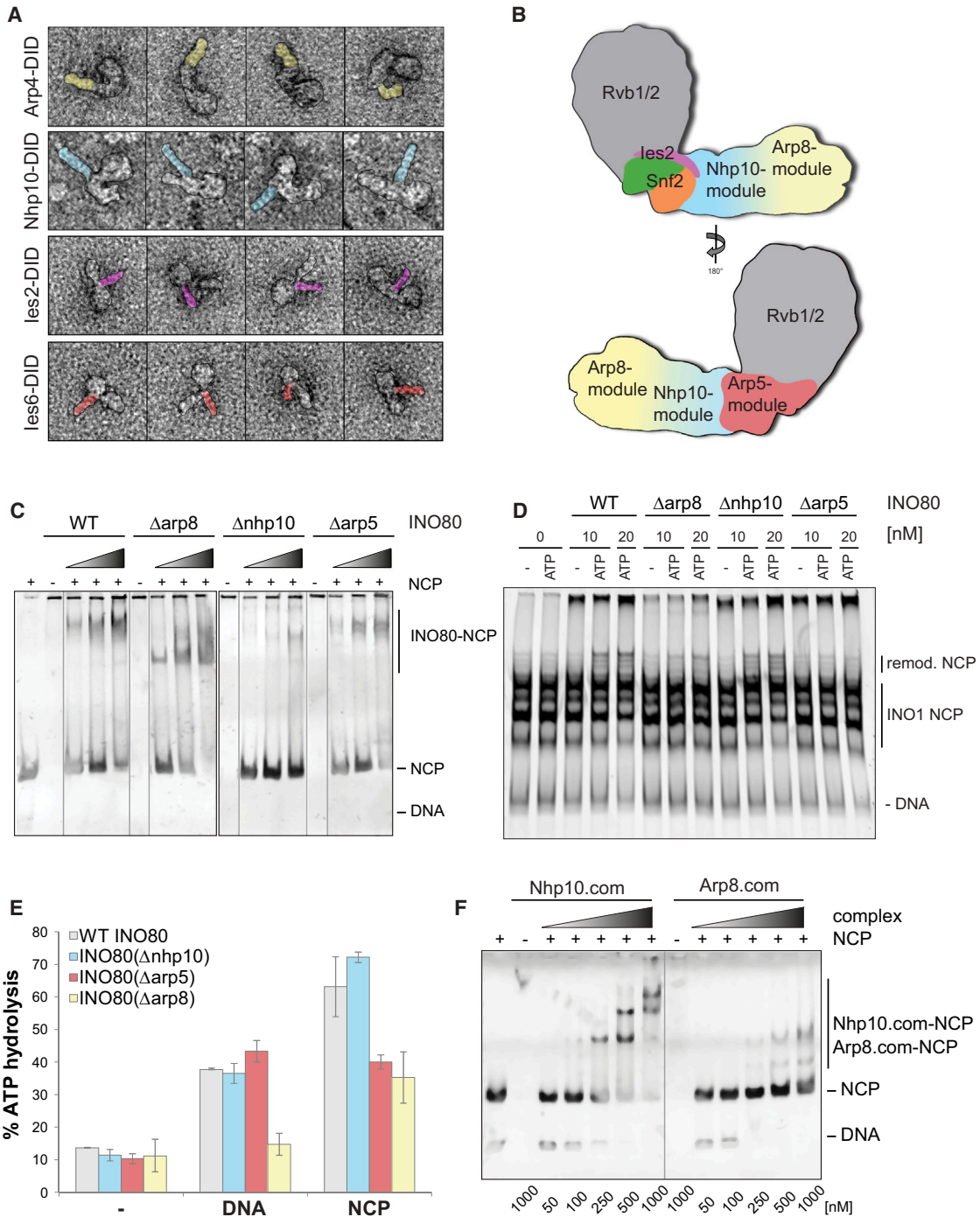

Figure 5. Assignment of Module Position and Function

(A) Localization of INO80 modules by DID labeling of a representative subunit and negative-stain EM of purified INO80 complexes. The DID-tag (yellow) on Arp4 protrudes out at the foot of INO80. The DID-tag (blue) on Nhp10 protrudes out at the body of INO80. The DID-tag of Ies6 (red) and Ies2 (pink) protrude at the neck of INO80.

(B) The Rvb1/2 complex (gray) is located in the head of INO80. The Snf2 ATPase (RecA1, orange; RecA2, green) in the neck is crowned by Ies2 (pink) and has the Arp5 module on the back (red). The Nhp10 module is assigned to the body (blue), and the Arp8 module is assigned to the foot (yellow).

(C) In gel mobility shift assays with increasing concentrations of INO80 complexes. INO80(Δarp5) and INO80(Δarp8) bound nucleosomes (NCP) marginally less efficiently compared to WT INO80. INO80(Δnhp10) showed reduced binding. Black lines separate different gels; gray lines separate lanes from the same gel.

(D) INO80 remodeled INO1 nucleosomes in an ATP-dependent manner. INO80(Δnhp10) was able to slide, whereas remodeling of INO80(Δarp8) was reduced and INO80(Δarp5) could not remodel.

(legend continued on next page)

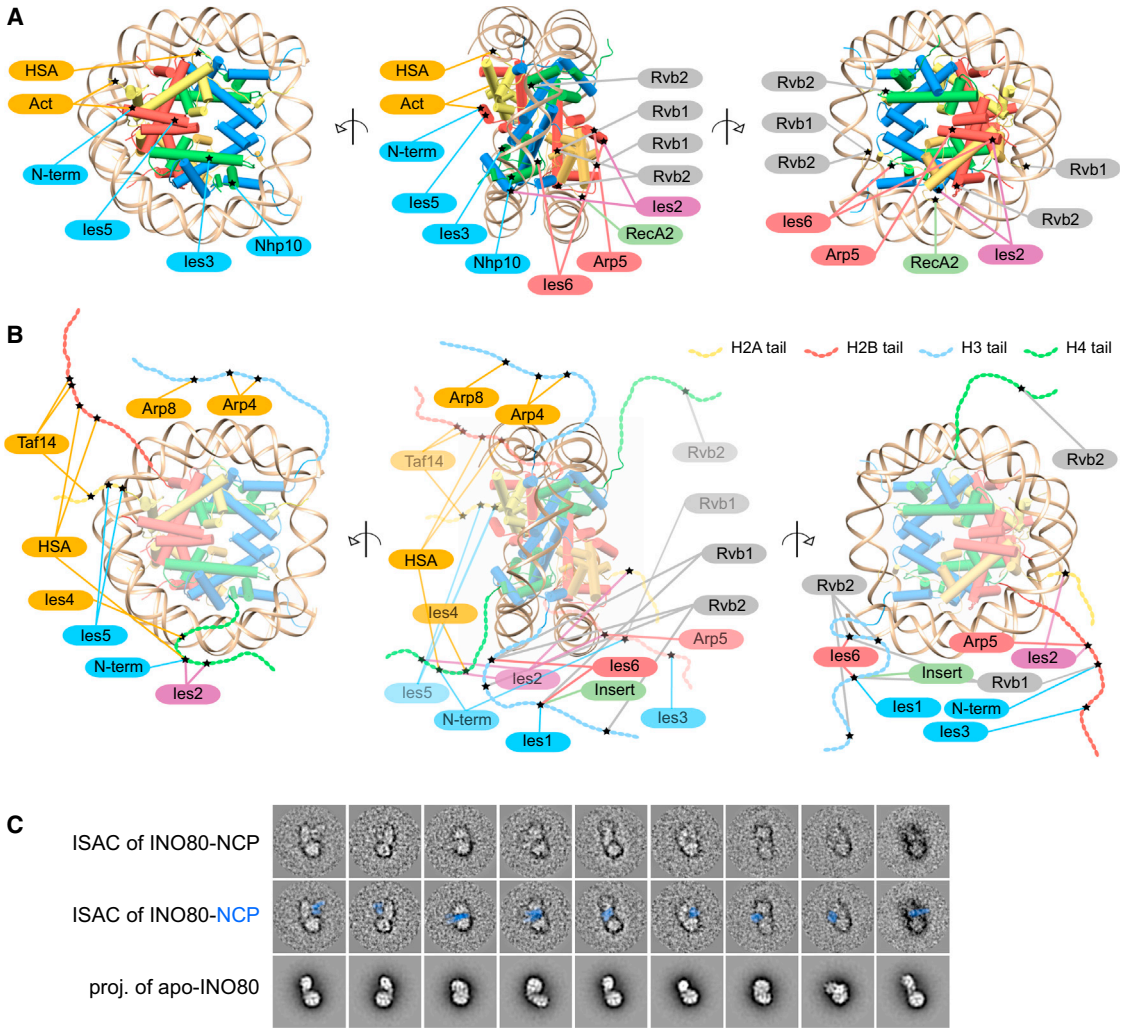

Figure 6. Topological Map of an INO80 Nucleosome Complex

(A and B) XL-MS analysis of INO80 nucleosome complex showed that one side of the nucleosome (PDB ID code 2PYO; Clapier et al., 2008) was crosslinking to INO80 subunits of the head (gray, pink, and green) and neck (red) and the other side to modules of the body (blue) and foot (yellow). (A) Tight constraints were imposed by crosslinks to structured histone residues and (B) loose restraints by crosslinks in remote N-terminal tail residues.

(C) Comparison of stable class averages from ISAC of negatively stained INO80 nucleosome complexes with projections of apo INO80 reveal additional density (blue) that could be assigned to the nucleosome.

See also Figure S5 and Table S6.

nucleosome core with the Snf2 domain and bind extranucleosomal DNA with the HAND-SANT-SLIDE (HSS) domain and accessory subunits (Racki et al., 2009; Yamada et al., 2011), suggesting a yet different mode of interaction.

We can position the nucleosome in the concave surface patch between head, body, and foot that is consistent with an involvement of all INO80 modules in nucleosome binding. In order to fulfill several distance restraints identified between the nucleosome and INO80 subunits, the distal foot of INO80 probably has to fold back to grasp the nucleosome. We indeed find this conformational flexibility by EM. In summary, our results suggest that INO80 has a distinct mechanism of interacting with the nucleosome by forming a flexible cradle that could partially embrace the nucleosome.

(E) INO80 WT and deletion mutants showed intrinsic ATPase activity (data are represented as mean ± SEM). Presence of DNA stimulated the ATPase activity of INO80 WT; INO80(Δnhp10) and INO80(Δarp5), but not of INO80(Δarp8). Nucleosomes further stimulated the ATPase activity of INO80 WT and INO80(Δnhp10), but not of INO80(Δarp5). The ATP hydrolysis rate of INO80(Δarp8) was enhanced by nucleosomes up to DNA-stimulated INO80 WT levels.

(F) Recombinant Nhp10-Ies3-Ies5 (Nhp10.com) and HSA-Act-Arp4-Arp8 (Arp8.com) showed high affinity to the NCP, and both complexes oligomerize with the NCP. Gray lines separate lanes from the same gel.

See also Figure S4.

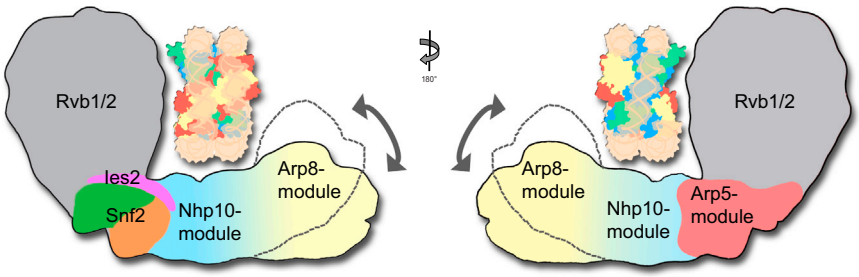

Figure 7. Proposed Nucleosome Remodeling Mechanism of INO80

The nucleosome is sandwiched between the head and the foot of INO80. The flexible foot could fold back and thus promote remodeling of the nucleosome. DNA-binding proteins are in place to coordinate this reaction.

A prominent feature of INO80 is the head that harbors the Rvb1/2 complex. The functional role of Rvb1/2 in chromatin remodelers and other complexes is still unknown, although they are essential for chromatin remodeling by INO80 (Jónsson et al., 2004). Given its peripheral location, a situation in which Rvb1/2 acts as a scaffold or is involved in the assembly of INO80 itself is unlikely. Isolated Rvb1/2 dodecamers can undergo large conformational changes that result in movements of domain 2, a condition that was suggested to influence DNA binding (López-Perrote et al., 2012; Petukhov et al., 2012). Our results placed the DNA-binding OB folds in close proximity to the Snf2 domain, suggesting that conformational changes in Rvb1/2 might either directly cooperate with the Snf2 motor in nucleosome remodeling or histone variant exchange, or could help to modulate the interaction of INO80 with chromatin.

Whereas the function of Rvb1/2 needs to be addressed in future studies, our data clarify its structure in INO80. The architecture of Rvb1/2 has been controversially discussed and our data support an arrangement of two heterohexameric Rvb1/2 rings stacked via the OB fold domains, in line with data on isolated Rvb1/2 (Gorynia et al., 2011; López-Perrote et al., 2012; Torreira et al., 2008). However, we observe also structural differences between Rvb1/2 within the INO80 complex and isolated Rvb1/2; thus, Rvb1/2 could be trapped in a particular conformation in INO80. Although, we detect an overall 6-fold symmetry in the head, a closer inspection of the cryo-EM density shows deviation from a strict rotational 6-fold symmetry at the Rvb1/2 OB folds close to the neck of the INO80 complex. This deviation may be a consequence of the interactions with the Snf2 ATPase of Ino80 (and its insert) and possibly other subunits, and explains the 1:1 interaction of Ino80 with Rvb1/2 dodecamers.

The Arp5-Ies6 module at the neck, backed on the Snf2 ATPase, is in close proximity to Rvb1/2. The homologous subunit of Ies6 in SWR1 (Swc2) has been proposed to act as a H2A.Z/H2B chaperone (Mizuguchi et al., 2004; Wu et al., 2005). Studies from us and others suggest that the function of the Arp5 module is essential for nucleosome-stimulated ATP hydrolysis and chromatin remodeling (Figures 5D and 5E) (Shen et al., 2003), supporting the idea of the Arp5 module functioning as a nucleosome/histone chaperone complex and remodeling facilitator that associates with histones.

The structural arrangement of the HSA^{Ino80}-Act-Arp4-Arp8 could in part resemble the Arp7-Arp9 dimer described in the HSA^{Snf2}-Arp7-Arp9-Rtt102 subcomplex of SWI/SNF (Schubert et al., 2013). Our XL-MS and EM data are consistent with the elongated α-helical conformation of the HSA domain that would span the interface of actin-Arp4-Arp8 in INO80.

Unexpectedly, the nonconserved Nhp10 module was found at the body of the complex, in close proximity to Ino80's ATPase. Proteins of the Nhp10 module (Nhp10, Ies1, Ies3, and Ies5) have no detectable sequence homologs in, e.g., human and fly INO80, although future high-resolution structural studies might reveal fold conservation. Consistent with this central location, we show that the Nhp10 module of INO80 is a high-affinity nucleosome-binding module. Nhp10 is an HMG2-box protein known to bind distorted DNA (Ray and Grove, 2009, 2012), rendering Nhp10 an ideal candidate for binding the bent nucleosomal DNA. It is thus plausible that the Nhp10 module interacts with nucleosomal DNA at the vicinity of the Snf2 domain. Attenuation of remodeling, but no impact on the ATP hydrolysis, raises the possibility that the Nhp10 module facilitates nucleosome sliding by binding to reaction intermediate states.

The location of structural modules on the basis of EM and XL-MS analysis and the observed conformational flexibility and interaction with the nucleosome suggests a cradle model for INO80 as depicted in Figure 7. A nucleosome could be sandwiched between head and foot, with the nucleosomal DNA oriented toward the neck and body. Arps in Arp8 and Arp5 modules could help binding to histones at both sides of the nucleosome. Such a plausible and testable model is consistent with other studies that show that Arp4 and Arp8 (foot) bind histones (Gerhold et al., 2012; Harata et al., 1999; Shen et al., 2003) and Snf2 domains (neck) (Dürr et al., 2005; Hauk et al., 2010; Thomä et al., 2005), Rvb1/2 OB domains (head) (Matias et al., 2006), and Nhp10 (body) (Ray and Grove, 2009, 2012) bind DNA. Such an enclosure might explain how INO80 acquires the ability to space nucleosomes (Udugama et al., 2011) by acting as a steric ruler as also suggested for ISWI (Yamada et al., 2011). The large conformational changes in INO80 could be relevant for remodeling by promoting "open" nucleosome conformations (Böhm et al., 2011) as reviewed in Andrews and Luger (2011). In open nucleosome conformations H2A-H2B dimers are partially dissociated from the H3-H4 tetramer, which would facilitate H2A histone variant exchange. A partially opened nucleosome could also explain why we find crosslinks to lysines that are buried in a closed nucleosome.

We provide a structural and functional framework for the INO80 complex in chromatin remodeling and histone variant exchange. Our results are a considerable step forward in the structural understanding of these large and flexible macromolecular machines and serve as framework to address the mechanism of the remodeling reaction by INO80 family remodels in future studies.

EXPERIMENTAL PROCEDURES

Electron Microscopy

Proteins were purified in accordance with standard methods (see Extended Experimental Procedures). INO80 was stabilized with glutaraldehyde and subjected to negative staining with 2% uranyl acetate or vitrified using a Vitrobot Mark IV (FEI Company). Negatively stained micrographs were recorded on a Tecnai G2 Spirit TEM at 120 kV. For cryo-EM, visualization was performed by a Titan Krios TEM (FEI Company) at 200 kV.

Data Processing

For negative staining, particle selection, initial image processing, class averaging, and initial model reconstruction were performed using EMAN2 (Tang et al., 2007). The EMAN2 model was subjected to SPIDER (Frank et al., 1996) for iterative projection matching and back projection. After sorting, the final resolution of 22 Å was estimated based on the Fourier shell correlation (FSC) at 0.5. Reference-free class averaging was repeated with ISAC (Yang et al., 2012), and ISAC classes were correlated to projections of the INO80 structure using SPIDER.

Using the negative-stain structure as a reference, cryo-EM data were processed with the SPIDER software package in principal analogous to Becker et al. (2012). INO80 refined to a final resolution of 17.5 Å (FSC = 0.5).

Crosslinking and Mass Spectrometry

INO80 and INO80 nucleosome complexes were crosslinked with isotope-labeled DSS. Crosslinked peptides were enriched using size-exclusion chromatography, analyzed on a liquid chromatography tandem mass spectrometer, and identified by xQuest (Rinner et al., 2008; Walzthoeni et al., 2012). Crosslinking procedure, MS analysis, and database searching were performed as described before (Herzog et al., 2012).

Biochemical Assays

Complexes were incubated with nucleosomes and analyzed by native PAGE. ATPase reactions were either stimulated by DNA or by nucleosomes.

Localization of Subunits

A DID1 tag was fused to Arp4, Nhp10, Ies6, and Ies2 in a *dyn2*Δ INO80-FLAG strain. The DID-tag was assembled by incubation with DID2 and Dyn2 (Flemming et al., 2010). DID-tagged INO80 complexes were enriched and purified, and the EM samples were prepared as described.

ACCESSION NUMBERS

The EMDataBank accession codes for the negative stain and cryo-EM map reported in this paper are EMB-2385 and EMD-2386, respectively.

SUPPLEMENTAL INFORMATION

Supplemental Information includes Extended Experimental Procedures, five figures, and six tables and can be found with this article online at http://dx.doi.org/10.1016/j.cell.2013.08.016.

ACKNOWLEDGMENTS

This project was funded by the German Research Council (GRK1721, SFB 646, and SFB/TR5) and the Center for Integrated Protein Science (to K.-P.H. and R.B.). K.-P.H. acknowledges support by the European Research Council (advanced grant ATMMACHINE). F.H. and K.P.H acknowledge support by the BioSysNet. C.H. was supported by the Ernst Schering Foundation. F.H. was supported by the European Molecular Biology Organization (long-term fellowship) and by the European Commission (FP7-PEOPLE-IEF); R.A. and F.H. were supported in part by the EU FP7 project PROSPECTS; and R.A. was supported by European Research Council advanced grant Proteomics v. 3.0 (233226). We thank the Becker's lab for plasmids and protocols for nucleosome reconstitution and the Hurt's lab for plasmids for DID labeling. The INO80-FLAG strain was a kind gift from the Shen lab. We thank the Cramer's and Thomm's group for fermentation.

Received: March 4, 2013
Revised: June 5, 2013
Accepted: August 12, 2013
Published: September 12, 2013

REFERENCES

Andrews, A.J., and Luger, K. (2011). Nucleosome structure(s) and stability: variations on a theme. Annu. Rev. Biophys. *40*, 99–117.

Asturias, F.J., Chung, W.H., Kornberg, R.D., and Lorch, Y. (2002). Structural analysis of the RSC chromatin-remodeling complex. Proc. Natl. Acad. Sci. USA *99*, 13477–13480.

Becker, T., Franckenberg, S., Wickles, S., Shoemaker, C.J., Anger, A.M., Armache, J.P., Sieber, H., Ungewickell, C., Berninghausen, O., Daberkow, I., et al. (2012). Structural basis of highly conserved ribosome recycling in eukaryotes and archaea. Nature *482*, 501–506.

Billon, P., and Côté, J. (2012). Precise deposition of histone H2A.Z in chromatin for genome expression and maintenance. Biochim. Biophys. Acta *1819*, 290–302.

Böhm, V., Hieb, A.R., Andrews, A.J., Gansen, A., Rocker, A., Tóth, K., Luger, K., and Langowski, J. (2011). Nucleosome accessibility governed by the dimer/tetramer interface. Nucleic Acids Res. *39*, 3093–3102.

Chaban, Y., Ezeokonkwo, C., Chung, W.H., Zhang, F., Kornberg, R.D., Maier-Davis, B., Lorch, Y., and Asturias, F.J. (2008). Structure of a RSC-nucleosome complex and insights into chromatin remodeling. Nat. Struct. Mol. Biol. *15*, 1272–1277.

Chen, L., Cai, Y., Jin, J., Florens, L., Swanson, S.K., Washburn, M.P., Conaway, J.W., and Conaway, R.C. (2011). Subunit organization of the human INO80 chromatin remodeling complex: an evolutionarily conserved core complex catalyzes ATP-dependent nucleosome remodeling. J. Biol. Chem. *286*, 11283–11289.

Clapier, C.R., and Cairns, B.R. (2009). The biology of chromatin remodeling complexes. Annu. Rev. Biochem. *78*, 273–304.

Clapier, C.R., Chakravarthy, S., Petosa, C., Fernández-Tornero, C., Luger, K., and Müller, C.W. (2008). Structure of the Drosophila nucleosome core particle highlights evolutionary constraints on the H2A-H2B histone dimer. Proteins *71*, 1–7.

Dang, W., and Bartholomew, B. (2007). Domain architecture of the catalytic subunit in the ISW2-nucleosome complex. Mol. Cell. Biol. *27*, 8306–8317.

Dechassa, M.L., Zhang, B., Horowitz-Scherer, R., Persinger, J., Woodcock, C.L., Peterson, C.L., and Bartholomew, B. (2008). Architecture of the SWI/SNF-nucleosome complex. Mol. Cell. Biol. *28*, 6010–6021.

Downs, J.A., Allard, S., Jobin-Robitaille, O., Javaheri, A., Auger, A., Bouchard, N., Kron, S.J., Jackson, S.P., and Côté, J. (2004). Binding of chromatin-modifying activities to phosphorylated histone H2A at DNA damage sites. Mol. Cell *16*, 979–990.

Dürr, H., Körner, C., Müller, M., Hickmann, V., and Hopfner, K.P. (2005). X-ray structures of the Sulfolobus solfataricus SWI2/SNF2 ATPase core and its complex with DNA. Cell *121*, 363–373.

Fenn, S., Breitsprecher, D., Gerhold, C.B., Witte, G., Faix, J., and Hopfner, K.P. (2011). Structural biochemistry of nuclear actin-related proteins 4 and 8 reveals their interaction with actin. EMBO J. *30*, 2153–2166.

Flemming, D., Thierbach, K., Stelter, P., Böttcher, B., and Hurt, E. (2010). Precise mapping of subunits in multiprotein complexes by a versatile electron microscopy label. Nat. Struct. Mol. Biol. *17*, 775–778.

Gerhold, C.B., Winkler, D.D., Lakomek, K., Seifert, F.U., Fenn, S., Kessler, B., Witte, G., Luger, K., and Hopfner, K.P. (2012). Structure of Actin-related protein 8 and its contribution to nucleosome binding. Nucleic Acids Res. *40*, 11036–11046.

Gorynia, S., Bandeiras, T.M., Pinho, F.G., McVey, C.E., Vonrhein, C., Round, A., Svergun, D.I., Donner, P., Matias, P.M., and Carrondo, M.A. (2011). Structural and functional insights into a dodecameric molecular machine - the RuvBL1/RuvBL2 complex. J. Struct. Biol. *176*, 279–291.

Harata, M., Oma, Y., Mizuno, S., Jiang, Y.W., Stillman, D.J., and Wintersberger, U. (1999). The nuclear actin-related protein of Saccharomyces cerevisiae, Act3p/Arp4, interacts with core histones. Mol. Biol. Cell *10*, 2595–2605.

Hauk, G., McKnight, J.N., Nodelman, I.M., and Bowman, G.D. (2010). The chromodomains of the Chd1 chromatin remodeler regulate DNA access to the ATPase motor. Mol. Cell *39*, 711–723.

Herzog, F., Kahraman, A., Boehringer, D., Mak, R., Bracher, A., Walzthoeni, T., Leitner, A., Beck, M., Hartl, F.U., Ban, N., et al. (2012). Structural probing of a protein phosphatase 2A network by chemical cross-linking and mass spectrometry. Science *337*, 1348–1352.

Hopfner, K.P., Gerhold, C.B., Lakomek, K., and Wollmann, P. (2012). Swi2/Snf2 remodelers: hybrid views on hybrid molecular machines. Curr. Opin. Struct. Biol. *22*, 225–233.

Jha, S., and Dutta, A. (2009). RVB1/RVB2: running rings around molecular biology. Mol. Cell *34*, 521–533.

Jónsson, Z.O., Jha, S., Wohlschlegel, J.A., and Dutta, A. (2004). Rvb1p/Rvb2p recruit Arp5p and assemble a functional Ino80 chromatin remodeling complex. Mol. Cell *16*, 465–477.

Kapoor, P., Chen, M., Winkler, D.D., Luger, K., and Shen, X. (2013). Evidence for monomeric actin function in INO80 chromatin remodeling. Nat. Struct. Mol. Biol. *20*, 426–432.

Leschziner, A.E. (2011). Electron microscopy studies of nucleosome remodelers. Curr. Opin. Struct. Biol. *21*, 709–718.

Leschziner, A.E., Lemon, B., Tjian, R., and Nogales, E. (2005). Structural studies of the human PBAF chromatin-remodeling complex. Structure *13*, 267–275.

Leschziner, A.E., Saha, A., Wittmeyer, J., Zhang, Y., Bustamante, C., Cairns, B.R., and Nogales, E. (2007). Conformational flexibility in the chromatin remodeler RSC observed by electron microscopy and the orthogonal tilt reconstruction method. Proc. Natl. Acad. Sci. USA *104*, 4913–4918.

Li, Z., Gadue, P., Chen, K., Jiao, Y., Tuteja, G., Schug, J., Li, W., and Kaestner, K.H. (2012). Foxa2 and H2A.Z mediate nucleosome depletion during embryonic stem cell differentiation. Cell *151*, 1608–1616.

López-Perrote, A., Muñoz-Hernández, H., Gil, D., and Llorca, O. (2012). Conformational transitions regulate the exposure of a DNA-binding domain in the RuvBL1-RuvBL2 complex. Nucleic Acids Res. *40*, 11086–11099.

Matias, P.M., Gorynia, S., Donner, P., and Carrondo, M.A. (2006). Crystal structure of the human AAA+ protein RuvBL1. J. Biol. Chem. *281*, 38918–38929.

Mizuguchi, G., Shen, X., Landry, J., Wu, W.H., Sen, S., and Wu, C. (2004). ATP-driven exchange of histone H2AZ variant catalyzed by SWR1 chromatin remodeling complex. Science *303*, 343–348.

Morrison, A.J., and Shen, X. (2009). Chromatin remodelling beyond transcription: the INO80 and SWR1 complexes. Nat. Rev. Mol. Cell Biol. *10*, 373–384.

Morrison, A.J., Highland, J., Krogan, N.J., Arbel-Eden, A., Greenblatt, J.F., Haber, J.E., and Shen, X. (2004). INO80 and gamma-H2AX interaction links ATP-dependent chromatin remodeling to DNA damage repair. Cell *119*, 767–775.

Morrison, A.J., Kim, J.A., Person, M.D., Highland, J., Xiao, J., Wehr, T.S., Hensley, S., Bao, Y., Shen, J., Collins, S.R., et al. (2007). Mec1/Tel1 phosphorylation of the INO80 chromatin remodeling complex influences DNA damage checkpoint responses. Cell *130*, 499–511.

Papamichos-Chronakis, M., and Peterson, C.L. (2008). The Ino80 chromatin-remodeling enzyme regulates replisome function and stability. Nat. Struct. Mol. Biol. *15*, 338–345.

Papamichos-Chronakis, M., and Peterson, C.L. (2013). Chromatin and the genome integrity network. Nat. Rev. Genet. *14*, 62–75.

Papamichos-Chronakis, M., Watanabe, S., Rando, O.J., and Peterson, C.L. (2011). Global regulation of H2A.Z localization by the INO80 chromatin-remodeling enzyme is essential for genome integrity. Cell *144*, 200–213.

Petukhov, M., Dagkessamanskaja, A., Bommer, M., Barrett, T., Tsaneva, I., Yakimov, A., Quéval, R., Shvetsov, A., Khodorkovskiy, M., Käs, E., and Grigoriev, M. (2012). Large-scale conformational flexibility determines the properties of AAA+ TIP49 ATPases. Structure *20*, 1321–1331.

Puri, T., Wendler, P., Sigala, B., Saibil, H., and Tsaneva, I.R. (2007). Dodecameric structure and ATPase activity of the human TIP48/TIP49 complex. J. Mol. Biol. *366*, 179–192.

Racki, L.R., Yang, J.G., Naber, N., Partensky, P.D., Acevedo, A., Purcell, T.J., Cooke, R., Cheng, Y., and Narlikar, G.J. (2009). The chromatin remodeller ACF acts as a dimeric motor to space nucleosomes. Nature *462*, 1016–1021.

Ray, S., and Grove, A. (2009). The yeast high mobility group protein HMO2, a subunit of the chromatin-remodeling complex INO80, binds DNA ends. Nucleic Acids Res. *37*, 6389–6399.

Ray, S., and Grove, A. (2012). Interaction of Saccharomyces cerevisiae HMO2 domains with distorted DNA. Biochemistry *51*, 1825–1835.

Rinner, O., Seebacher, J., Walzthoeni, T., Mueller, L.N., Beck, M., Schmidt, A., Mueller, M., and Aebersold, R. (2008). Identification of cross-linked peptides from large sequence databases. Nat. Methods *5*, 315–318.

Saravanan, M., Wuerges, J., Bose, D., McCormack, E.A., Cook, N.J., Zhang, X., and Wigley, D.B. (2012). Interactions between the nucleosome histone core and Arp8 in the INO80 chromatin remodeling complex. Proc. Natl. Acad. Sci. USA *109*, 20883–20888.

Schubert, H.L., Wittmeyer, J., Kasten, M.M., Hinata, K., Rawling, D.C., Héroux, A., Cairns, B.R., and Hill, C.P. (2013). Structure of an actin-related subcomplex of the SWI/SNF chromatin remodeler. Proc. Natl. Acad. Sci. USA *110*, 3345–3350.

Schulze, J.M., Kane, C.M., and Ruiz-Manzano, A. (2010). The YEATS domain of Taf14 in Saccharomyces cerevisiae has a negative impact on cell growth. Mol. Genet. Genomics *283*, 365–380.

Seeber, A., Hauer, M., and Gasser, S.M. (2013). Nucleosome remodelers in double-strand break repair. Curr. Opin. Genet. Dev. *23*, 174–184.

Shen, X., Mizuguchi, G., Hamiche, A., and Wu, C. (2000). A chromatin remodelling complex involved in transcription and DNA processing. Nature *406*, 541–544.

Shen, X., Ranallo, R., Choi, E., and Wu, C. (2003). Involvement of actin-related proteins in ATP-dependent chromatin remodeling. Mol. Cell *12*, 147–155.

Skiniotis, G., Moazed, D., and Walz, T. (2007). Acetylated histone tail peptides induce structural rearrangements in the RSC chromatin remodeling complex. J. Biol. Chem. *282*, 20804–20808.

Smith, C.L., Horowitz-Scherer, R., Flanagan, J.F., Woodcock, C.L., and Peterson, C.L. (2003). Structural analysis of the yeast SWI/SNF chromatin remodeling complex. Nat. Struct. Biol. *10*, 141–145.

Szerlong, H., Hinata, K., Viswanathan, R., Erdjument-Bromage, H., Tempst, P., and Cairns, B.R. (2008). The HSA domain binds nuclear actin-related proteins to regulate chromatin-remodeling ATPases. Nat. Struct. Mol. Biol. *15*, 469–476.

Tang, G., Peng, L., Baldwin, P.R., Mann, D.S., Jiang, W., Rees, I., and Ludtke, S.J. (2007). EMAN2: an extensible image processing suite for electron microscopy. J. Struct. Biol. *157*, 38–46.

Thomä, N.H., Czyzewski, B.K., Alexeev, A.A., Mazin, A.V., Kowalczykowski, S.C., and Pavletich, N.P. (2005). Structure of the SWI2/SNF2 chromatin-remodeling domain of eukaryotic Rad54. Nat. Struct. Mol. Biol. *12*, 350–356.

Torreira, E., Jha, S., López-Blanco, J.R., Arias-Palomo, E., Chacón, P., Cañas, C., Ayora, S., Dutta, A., and Llorca, O. (2008). Architecture of the pontin/reptin complex, essential in the assembly of several macromolecular complexes. Structure *16*, 1511–1520.

Udugama, M., Sabri, A., and Bartholomew, B. (2011). The INO80 ATP-dependent chromatin remodeling complex is a nucleosome spacing factor. Mol. Cell. Biol. *31*, 662–673.

van Attikum, H., Fritsch, O., Hohn, B., and Gasser, S.M. (2004). Recruitment of the INO80 complex by H2A phosphorylation links ATP-dependent chromatin remodeling with DNA double-strand break repair. Cell *119*, 777–788.

Vorobiev, S., Strokopytov, B., Drubin, D.G., Frieden, C., Ono, S., Condeelis, J., Rubenstein, P.A., and Almo, S.C. (2003). The structure of nonvertebrate actin: implications for the ATP hydrolytic mechanism. Proc. Natl. Acad. Sci. USA *100*, 5760–5765.

Walzthoeni, T., Claassen, M., Leitner, A., Herzog, F., Bohn, S., Förster, F., Beck, M., and Aebersold, R. (2012). False discovery rate estimation for cross-linked peptides identified by mass spectrometry. Nat. Methods *9*, 901–903.

Wang, A.Y., Schulze, J.M., Skordalakes, E., Gin, J.W., Berger, J.M., Rine, J., and Kobor, M.S. (2009). Asf1-like structure of the conserved Yaf9 YEATS domain and role in H2A.Z deposition and acetylation. Proc. Natl. Acad. Sci. USA *106*, 21573–21578.

Wu, W.H., Alami, S., Luk, E., Wu, C.H., Sen, S., Mizuguchi, G., Wei, D., and Wu, C. (2005). Swc2 is a widely conserved H2AZ-binding module essential for ATP-dependent histone exchange. Nat. Struct. Mol. Biol. *12*, 1064–1071.

Yamada, K., Frouws, T.D., Angst, B., Fitzgerald, D.J., DeLuca, C., Schimmele, K., Sargent, D.F., and Richmond, T.J. (2011). Structure and mechanism of the chromatin remodelling factor ISW1a. Nature *472*, 448–453.

Yang, Z., Fang, J., Chittuluru, J., Asturias, F.J., and Penczek, P.A. (2012). Iterative stable alignment and clustering of 2D transmission electron microscope images. Structure *20*, 237–247.

Zhang, W., Zhang, J., Zhang, X., Xu, C., and Tu, X. (2011). Solution structure of the Taf14 YEATS domain and its roles in cell growth of Saccharomyces cerevisiae. Biochem. J. *436*, 83–90.